
E2E-SWIN-UNET++: AN ENHANCED END-TO-END SWIN-UNET ARCHITECTURE WITH DUAL DECODERS FOR PTMC SEGMENTATION

Maryam Dialameh

Department of Mechanical and Mechatronics Engineering
University of Waterloo, Waterloo, ON, Canada
maryam.dialameh@uwaterloo.ca

Hossein Rajabzadeh

Department of Mechanical and Mechatronics Engineering
University of Waterloo, Waterloo, ON, Canada
hossein.rajabzadeh@uwaterloo.ca

Moslem Sadeghi-Goughari

Department of Mechanical and Mechatronics Engineering
University of Waterloo, Waterloo, ON, Canada
m8sadegh@uwaterloo.ca

Jung Suk Sim

Department of Radiology
Withsim Clinic Seongnam, Korea
jungsuk.sim@gmail.com

Hyock Ju Kwon

Department of Mechanical and Mechatronics Engineering
University of Waterloo, Waterloo, ON, Canada
hjkwon@uwaterloo.ca

ABSTRACT

Efficiently managing papillary thyroid microcarcinoma (PTMC) while minimizing patient discomfort poses a significant clinical challenge. Radiofrequency ablation (RFA) offers a less invasive alternative to surgery and radiation therapy for PTMC treatment, characterized by shorter recovery times and reduced pain. As an image-guided procedure, RFA generates localized heat by delivering high-frequency electrical currents through electrodes to the targeted area under ultrasound imaging

guidance. However, the precision and skill required by operators for accurate guidance using current ultrasound B-mode imaging technologies remain significant challenges. To address these challenges, we develop a novel AI segmentation model, E2E-Swin-Unet++. This model enhances ultrasound B-mode imaging by enabling real-time identification and segmentation of PTMC tumors and monitoring of the region of interest for precise targeting during treatment. E2E-Swin-Unet++ is an advanced end-to-end extension of the Swin-Unet architecture, incorporating thyroid region information to minimize the risk of false PTMC segmentation while providing fast inference capabilities. Experimental results on a real clinical RFA dataset demonstrate the superior performance of E2E-Swin-Unet++ compared to related models. Our proposed solution significantly improves the precision and control of RFA ablation treatment by enabling real-time identification and segmentation of PTMC margins during the procedure.

1 Introduction

Papillary Thyroid Microcarcinoma (PTMC) is characterized by tumors that are 1 cm or smaller in diameter [1]. Despite its small size, PTMC can still pose significant health risks if not managed properly [2]. Radiofrequency Ablation (RFA) has emerged as a minimally invasive treatment option for PTMC treatment, particularly for patients who are not ideal candidates for open surgery [3]. RFA involves the use of high-frequency electrical currents to generate localized heat, effectively destroying cancer cells within the thyroid gland. During the RFA procedure, the physician relies on real-time ultrasound imaging to guide the ablation process [4]. However, this treatment faces two major challenges: 1) it becomes difficult for the physician to correctly identify the PTMC location and its boundaries; 2) distinguishing between normal tissue and a PTMC can be challenging in many cases [5].

Currently, ultrasound B-mode imaging is employed to guide RFA, allowing physicians to identify the tumor boundaries using images from the targeted area. Although ultrasound imaging offers a quick, cost-effective, and safe imaging solution, the precision of imaging and targeting, as well as the skill required from physicians, remain significant challenges [6]. First, ultrasound B-mode imaging suffers from limited resolution, which can lead to low accuracy in identifying tumor boundaries [7]. Additionally, during RFA treatment, each RF sonication generates microbubbles at the targeted area due to the ablation effect. These microbubbles can persist for minutes to hours, causing acoustic shadowing at the boundary of the PTMC. Consequently, subsequent sonications may face difficulties in accurately detecting the tumor boundary [8]. This can result in untreated tumor areas or necessitating repeated ablation procedures, increasing the risk of tissue overheating [9]. Despite advancements in medical imaging, the task of real-time targeting and tracking of the tumor area during RFA remains challenging, and clinicians continue to seek effective solutions for these issues.

Artificial Intelligence (AI), particularly deep learning (DL) models, has been successfully employed across various fields, including medical applications [10]. One of the most prominent uses of deep learning in the medical sector is medical image segmentation [11]. Such technologies are increasingly considered as valuable tools for assisting RFA

operators by providing real-time guidance and crucial insights during procedures. Unet, for instance, is a convolutional neural network architecture, and recognized as one of the primer and successful DL methods to tackle the problem of medical image segmentation. Variants of U-net such as V-net [12], U-net++ [13], attention U-net [14], residual U-net [15], and dense U-net [16] have been developed to overcome the limitations of the original U-net model, including faster convergence, the ability to handle varied segments sizes, and improving accuracy. A recent advantage of Medical SAM Adapter (Med-SAM) [17] adapts SAM framework for medical applications. The main idea of Med-SAM is applying low-rank adapters with ReLU activation to bridge the gap between SAM and medical segmentation tasks.

Another method, TRFE-Net [18], is an encoder-decode convolutional framework that incorporates prior knowledge of the thyroid region to enhance thyroid nodule segmentation accuracy in ultrasound images. Additionally, vision transformer-based architectures [19, 20] have opened up new possibilities for PTMC segmentation from ultrasound images. For instance, Swin- Unet [21] leverages the hierarchical nature of Swin-Transformers [22] to handle various scales of features effectively, enhancing performance in segmentation tasks.

Challenges in medical images, such as low pixel-intensity variations, class imbalance, organ interference and movement, and limited annotated samples, make this area of research particularly complex [23]. Moreover, current PTMC segmentation solutions for PTMC segmentation during RFA surgery face additional challenges, including the need for real-time prediction, robustness against organ movements in the throat region (as patients only receive regional anesthesia), and the ability to track PTMC amid bubbles created by heat during the procedure [24]. Another limitation of current state-of-the-art models is their inability to incorporate thyroid information into their predictions when dealing with PTMC segmentation using ultrasound images. For instance, we experimentally show that Swin-Unet exhibits a significant false positive rate in PTMC segmentation. Moreover, the information flow between a model’s layers play an important role in segmentation accuracies.

To address the above-mentioned limitations, we propose a novel segmentation model, named E2E-SWIN-UNET++, which is an end-to-end learning procedure built on the Swin-Unet model. More specifically, E2E-SWIN-UNET++ enhances segmentation accuracy by expanding the Swin-Unet model to incorporate two parallel decoders. The first decoder is designed to integrate the thyroid gland information, which is fed into the second decoder, leading to more precise segmentation results. By restricting the examination of PTMC to within the thyroid gland, we achieve two key benefits. Firstly, we minimize the risk of false positives by ensuring that predictions are confined to the thyroid gland. Secondly, we reduce the model’s search space, which allows it to focus on a smaller, more relevant region. This restriction not only simplifies the learning process but also results in a model with fewer parameters, thereby enhancing prediction speed during inference.

2 Proposed Method: E2E-Swin-Unet++

This section outlines our proposed model, E2E-Swin-Unet++, designed to address the task of PTMC segmentation from ultrasound images captured during RFA surgery. As illustrated in Figure 1 (a), the proposed E2E-Swin-Unet++

comprises one encoder and two decoders, each formed by stacking Swin-Unet blocks. The encoder receives the input grayscale patches of an ultrasound image captured during RFA surgery. These patches are first processed through a linear embedding layer, which transforms the raw pixel intensities into a sequence of tokens by splitting the image into 4×4 patches without overlap. Hence, each token at this stage is represented by a raw-intensity vector of size $4 \times 4 \times 1 = 16$. Subsequently, these patches are passed through a second linear embedding layer, converting raw-pixel patches to the embedding space of size C . The embedded tokens are passed through three pairs of Swin-Transformers blocks and patch merging layers, with the same functionality as the reference encoder in vanilla Swin-Unet [21]. The workflow of the Swin-Transformers block, illustrated in Figure 1-(b), consist of two successive self-attention sub-blocks. The first sub-block employs a windowed multi-head self-attention (W-MSA) along with layer normalization and GeLU-activated MLP modules, while the second sub-block uses a shifted-window multi-head self-attention (SW-MSA). The patch merging layers first normalize its input features and then reduce the spatial resolution by a factor of 2 while increasing the feature embedding size by a factor of 2. This process is computed through a linear projection operation. The encoder outputs are then passed to a bottleneck layer, comprising two consecutive Swin-Transformers layers.

The outputs of the bottleneck are directed towards two decoders: the first decoder predicts the thyroid gland segment, and the second decoder predicts the PTMC segment. Each decoder contains three layers, with each layer comprising a patch expanding module to up-sample the feature vector, a concatenation operator (depicted by \odot) to concatenate the patch expanding outputs with skip connections, a linear projection module, and finally a Swin-Transformers block. In both decoders, the linear projection modules are used to aggregate the concatenated features and maintain a consistent dimensions. Finally, a linear layer projects the decoders outputs to the generate pixel-level segmentation predictions.

While both decoders are similar to each other with the same architecture, they are different in terms of their input skip connections. Specifically, the first decoder receives the encoder’s intermediate features via skip connections. In contrast, the second decoder has access to information provided by the concatenated intermediate features of both the encoder and the first decoder. Therefore, the second decoder also has access to the information related to the thyroid gland, which further allows the second decoder to make more accurate predictions.

The proposed E2E-Swin-Unet++ is trained using an end-to-end (E2E) strategy. The training loss function consists of two components: 1) thyroid gland segmentation loss, and 2) PTMC segmentation loss. The first loss computes the prediction error for thyroid segmentation, while the second loss calculates the prediction error for PTMC segmentation. Equation 1 represents the training loss function, where α and β are hyper-parameters, $DL(\cdot)$ denotes Dice loss, and $BCE(\cdot)$ is the binary cross-entropy loss. Additionally, X represents the set of input samples, $F_1(X)$, $F_2(X)$ are the outputs of the first and second decoders, and Y_{PTMC} , $Y_{Thyroid}$ stand for the true labels for PTMCs and thyroids, respectively, associated with the inputs X .

$$Loss(X, Y_{Thyroid}, Y_{PTMC}) = \frac{1}{2} \left(\alpha \cdot BCE(F_1(X), Y_{Thyroid}) + (1 - \alpha) \cdot DL(F_1(X), Y_{Thyroid}) + \beta \cdot BCE(F_2(X), Y_{PTMC}) + (1 - \beta) \cdot DL(F_2(X), Y_{PTMC}) \right) \quad (1)$$

$$BCE(y, \hat{y}) = -\frac{1}{N} \sum_{i=1}^N \left(y_i \cdot \log(\hat{y}_i) + (1 - y_i) \cdot \log(1 - \hat{y}_i) \right) \quad (2)$$

$$Dice Loss(y, \hat{y}) = 1 - \frac{2 \sum_{i=1}^N y_i \hat{y}_i}{\sum_{i=1}^N y_i + \sum_{i=1}^N \hat{y}_i} \quad (3)$$

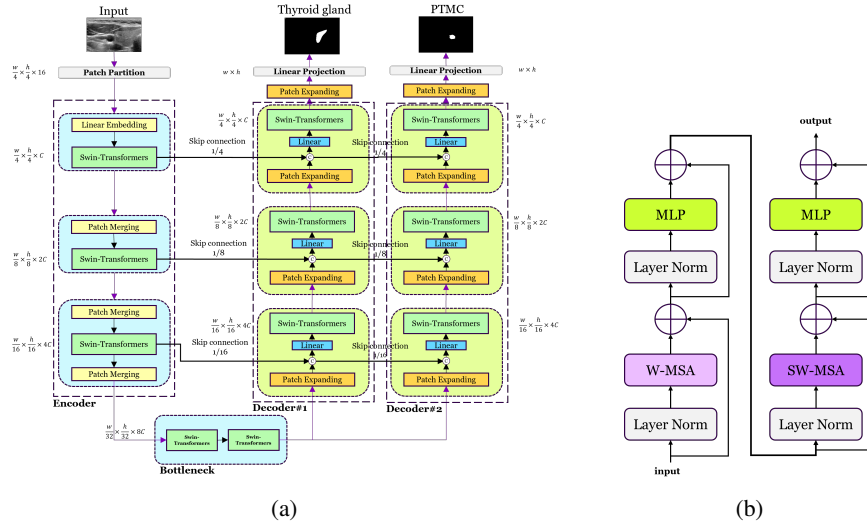


Figure 1: (a) The workflow diagram of the proposed E2E-Swin-Unet++. (b) The components of a Swin-Transformers layer used in E2E-Swin-Unet++.

Equation 2 and 3 respectively describe the BCE and DL losses, where y_i and \hat{y}_i are true label and the predicted probability, and N is the total number of samples.

3 Experiments

This section presents the evaluation and comparison results of our proposed E2E-Swin-Unet++ model against several relevant models. We utilized two datasets for the evaluation. The first dataset consists of 691 annotated ultrasound images collected from 101 anonymous patients who underwent RFA surgery. The dataset is divided into training, validation and test sets with proportions of 80%, 10%, 10%, respectively. The images are in jpg-format with a resolution of 786×531 pixels. We annotated them in collaboration with specialists, and all annotations were approved under their supervision. Figure 2 show sampled images from our dataset alongside their associated annotations.

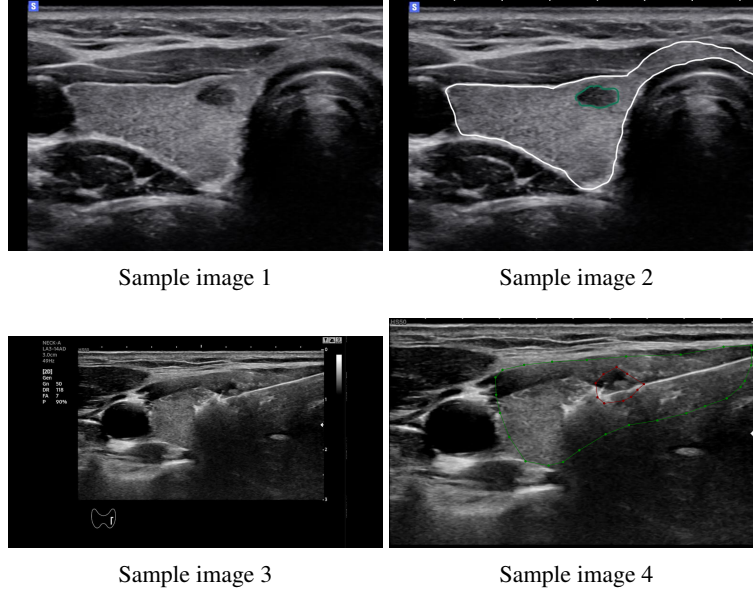


Figure 2: Sample ultrasound images from the dataset used in the experiments, along with their corresponding annotations. The images represent different instances of PTMC (Papillary Thyroid Microcarcinoma), highlighting the variability in appearance and the complexity of segmentation tasks.

The second dataset used for evaluation is TN3k [18], consisting of thyroid nodule images along with their associated masks. TN3K includes 3,493 ultrasound images collected from 2,421 cases. In the context of image segmentation, two commonly used evaluation metrics are the Jaccard Index and the Dice Coefficient. The Jaccard Index, also known as the Intersection over Union (IoU), is defined as the size of the intersection divided by the size of the union of the sample sets. Mathematically, it can be expressed as:

$$J(A, B) = \frac{|A \cap B|}{|A \cup B|} \quad (4)$$

where A and B present the ground truth and the predicted segmentation, respectively. The Jaccard Index ranges from 0 to 1, where 0 indicates no overlap and 1 indicates perfect overlap. The Dice Coefficient, also known as the Sørensen–Dice Index, is a statistic used to gauge the similarity between two samples. It is calculated as twice the size of the intersection divided by the sum of the sizes of the two sets. The formula for the Dice Coefficient is:

$$D(A, B) = \frac{2|A \cap B|}{|A| + |B|} \quad (5)$$

Similarly to the Jaccard Index, A and B represent the ground truth and the predicted segmentation. The Dice Coefficient also ranges from 0 to 1, where 0 means no overlap and 1 signifies a perfect match.

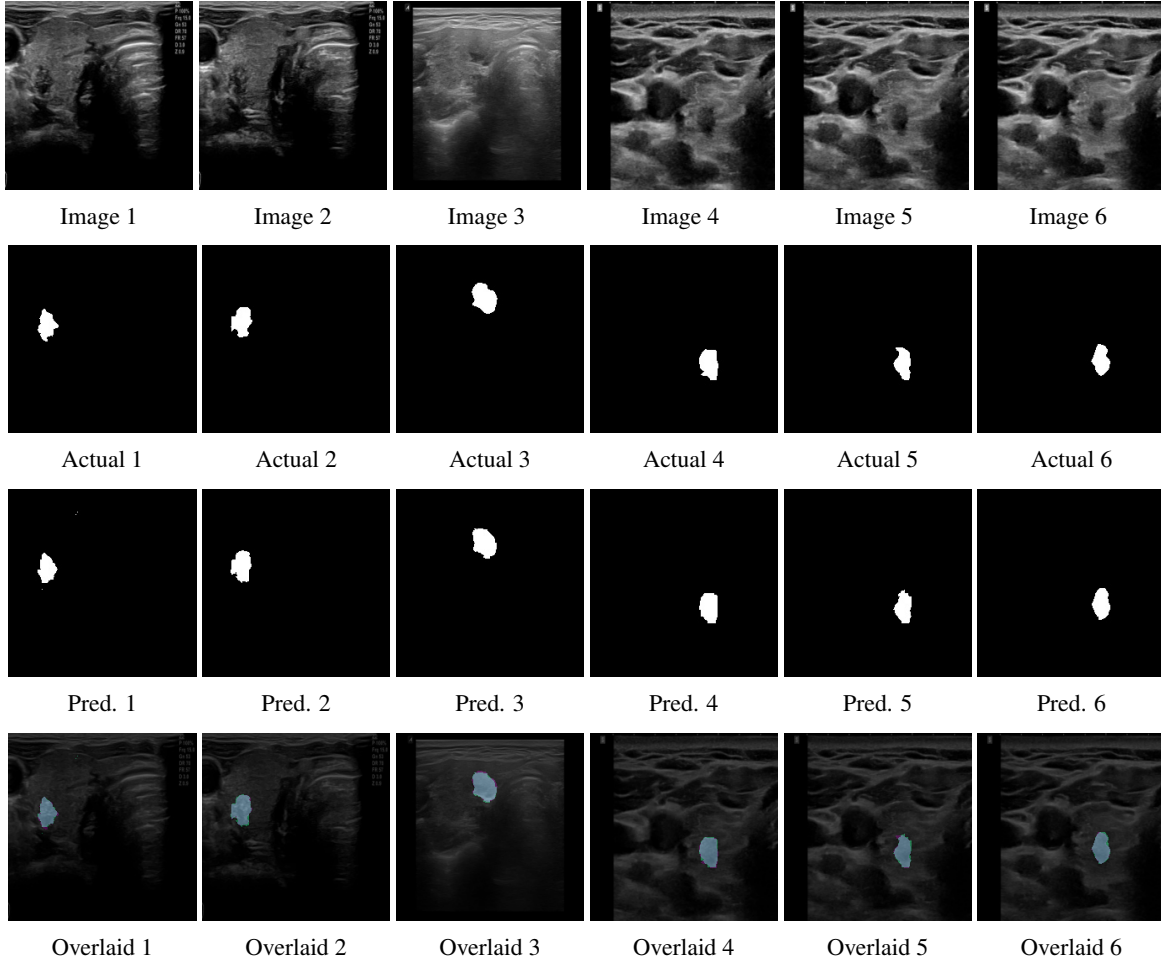


Figure 3: Evaluating the qualitative performance of E2E-Swin-Unet++. The first and the second rows show six randomly selected test instances along with their associated labels. Third row depicts the models’ prediction segmentation for each image, while the last row overlays the first three rows, in which the white, pink, and green areas indicate true positive, false negative, and false positive, respectively.

4 Results

4.1 Qualitative Evaluation

The first experiment visually evaluates the quality performance of E2E-Swin-Unet++ by using six randomly selected test instances from our collected dataset. Figure 3 illustrates the obtained results, consisting of six columns and four rows, where each column represents one image. The first and second rows display the original ultrasound images along with its actual PTMC labels. The third row shows the predicted PTMC segments generated by the model, while the fourth row overlays the first three rows to provide a comprehensive understanding of the model’s performance. In this overlay, white, pink, and green colors indicates true positive, false negative, and false positive, respectively. From these overlays, it is evident that the model performs with a high degree of accuracy, as the majority of the predicted segments closely align with the actual labels, demonstrating minimal false negatives and false positives. The consistency of the model’s

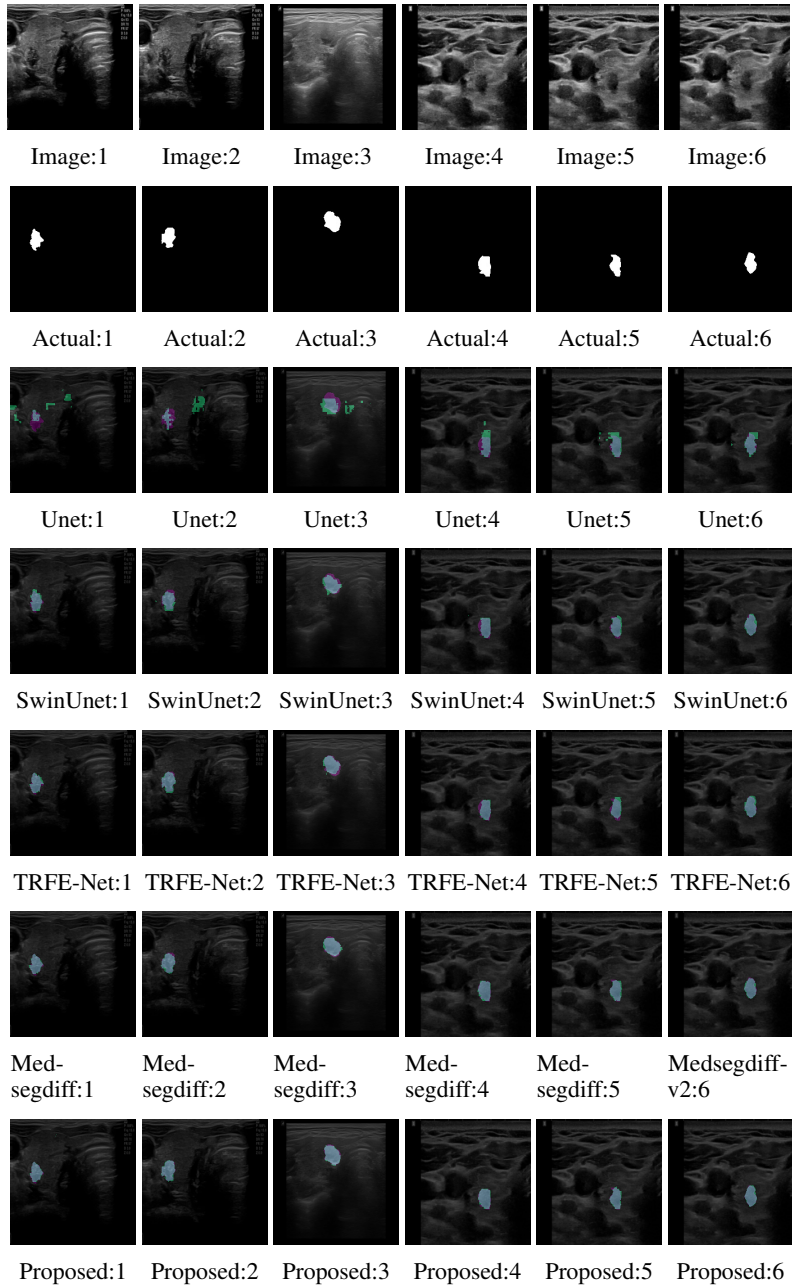


Figure 4: Qualitative comparison of overlaid segmentation results across several related models.

predictions across different images suggests its robustness in ability to generalize across various instances of PTMC within ultrasound imagery. Moreover, Figure 4 presents a qualitative comparison of overlaid segmentation results across several related models, including the proposed E2E-Swin-Unet++. The figure demonstrates that the proposed E2E-Swin-Unet++ model consistently produces segmentation results that align more closely with the actual PTMC labels, and demonstrates its superior performance by minimizing both false negatives and false positives, outperforming its counterparts in segmentation accuracy.

4.2 Quantitative Evaluation

Table 1 presents the numerical results obtained from the experiments ¹. E2E-Swint-Unet++ shows the highest performance, with a Jaccard index of 71.23% and a Dice coefficient of 84.36% on our dataset and a Jaccard of 69.14% and a Dice of 81.24% on the TN3K dataset. These results clearly demonstrate that E2E-Swint-Unet++ outperforms traditional models. The consistency in performance improvement across both datasets indicates the robustness of the advanced model designs under varying data scenarios and evaluation settings.

Table 1: Model performance comparison in terms of Dice and Jaccard scores. (Left) Results on our collected dataset. (Right) Results on the TN3K dataset. Each experiment is repeated three times and the average results are reported.

Model	Jaccard(%)	Dice(%)	Model	Jaccard(%)	Dice(%)
Unet	63.17	77.41	Unet	62.85	76.71
Unet ++	64.42	78.60	Unet ++	63.41	77.69
Swin-Unet	65.65	79.87	Swin-Unet	65.24	79.39
Swint-Unet++	67.20	82.15	Swint-Unet++	66.32	80.10
TRFE-Net	69.19	83.61	TRFE-Net	67.65	79.14
E2E-Swint-Unet++	71.23	84.36	E2E-Swint-Unet++	69.14	81.24

4.3 Speed and Efficiency Comparison

The second experiment evaluates the performance of E2E-Swin-Unet++ in both segmentation accuracy and prediction time per sample, comparing it with several state-of-the-art models, including nnUnet, Swin-UNetr, UNetr, SegDiff, and Medsegdiff-v2. As shown in Table 2, E2E-Swin-Unet++ achieves the highest Dice score of 83.36%, outperforming all other models in terms of segmentation accuracy. This result demonstrates the effectiveness of our model in leveraging thyroid gland information and utilizing dual decoders to enhance the PTMC segmentation. When it comes to prediction time, E2E-Swin-Unet++ provides a balance between accuracy and efficiency. With an average prediction time of 0.18 seconds per sample, it is slightly slower than nnUnet and Swin-UNetr but significantly faster than UNetr, SegDiff, and Medsegdiff-v2. This result indicates that E2E-Swin-Unet++ achieves superior segmentation performance without a significant trade-off in computational efficiency. Moreover, the prediction time of less than 0.2 seconds per sample highlights the potential of E2E-Swin-Unet++ model for online prediction tasks. This rapid inference capability makes it promising for use as an AI assistant during RFA surgery, where real-time decision support is critical.

Table 2: Comparison of models based on Dice scores on our collected dataset, along with the average prediction time per sample.

Model	Dice(%)	Average Prediction Time (seconds)
nnUnet	80.35	0.14 second
Swin-UNetr	81.16	0.15 second
UNetr	79.68	0.25 second
SegDiff	80.87	0.36 second
Medsegdiff-v2	80.68	0.31 second
E2E-Swin-Unet++	83.36	0.18 second

¹All experiments are conducted on the same hyper-parameter settings

Table 3: Impact of the number of skip connections on the performance of the E2E-Swin-Unet++ model. The table presents the results as the number of skip connections varies from 0 to 6, demonstrating how these changes affect the model’s performance.

	Our Dataset		TN3K	
	Jaccard	Dice	Jaccard	Dice
Skip Connections				
0	65.21	78.17	62.34	74.69
1	67.14	79.34	64.24	75.84
2	68.23	80.53	63.72	77.12
3	69.47	81.72	65.16	78.46
4	70.59	82.46	66.84	79.13
5	71.08	83.06	68.31	80.69
6	71.23	84.36	69.14	81.24

4.4 Ablation Study

This subsection explores the impact of different components of E2E-Swin-Unet++ on its segmentation performances. Specifically, we evaluate the effect of the first decoder, the types of skip connections and the number of skip connections on the model’s overall performance.

Impact of the first decoder: To evaluate the effectiveness of our proposed architecture, we assess the the effect of adding thyroid feature in E2E-Swint-Unet++. Specifically, we aim to understand how the first decoder enhances PTMC segmentation through the second decoder. To verify this, we removed the first decoder from the architecture and repeated the experiments outlined in Table 1. This change in the network downgrades the model to vanilla Swin-Unet. Interestingly, we observed a performance drop of 4.98% on our dataset and 3.11% on the TN3K benchmark. These results suggest that the inclusion of thyroid gland boundaries significantly enhances the model’s performance.

Impact of skip connections types: E2E-Swin-Unet++ employs Unet-like skip connections, where residual features are concatenated with current features and passed through a linear layer. This experiment explores the impact of using additive skip connections instead of concatenated ones. In this variation, residual features are added to the current features before passing them to the Swin-Transformers blocks. This modifications resulted in Dice score drops of 6.51% on our dataset and 5.11% on the TN3K benchmark. Hence, we conclude that the choice of Unet-like concatenated skip connections outperforms additive skip connections in this context.

Impact of the number of skip connections: E2E-Swin-Unet++ employs six skip connections, with two per each layer. This experiment evaluates the impact of varying the number of skip connections on the performance. Similar to Swin-Unet, we use three skip connections from the encoder to the first decoder and three additional connections from the first decoder to the second one. In this experiment, we vary the number of skip connections from 0 to 6 and report the results in Table 3. The results indicate that increasing the number of skip connections consistently improves the model’s performance, as evidenced by higher Jaccard and Dice scores on both our dataset and the TN3K benchmark. The highest performance is achieved with 6 skip connections.

5 Discussion

The proposed E2E-Swin-Unet++ model demonstrates significant promise for improving PTMC segmentation by incorporating thyroid gland information, leading to more accurate and efficient outcomes compared to existing models. The dual-decoder architecture effectively leverages thyroid features to enhance segmentation performance, as evidenced by the evaluation results. Ablation studies further validate the design choice, with substantial performance drops observed when thyroid feature integration is removed.

Limitations: This project comes with two primary limitations. First, while the model shows promise for PTMC segmentation, its generalizability to other types of thyroid cancers or medical conditions remains uncertain. Additional studies are required to assess its applicability and performance in other medical imaging tasks. Second, the evaluation was conducted on a relatively limited set of datasets. Although the results are promising, broader validation using more diverse and larger datasets is necessary to ensure the generalizability of the model across different populations and imaging conditions.

Future Direction: To address these limitations, future research should focus on implementing continuous learning mechanisms that allow the model to be periodically updated with new data and feedback from clinical use, thereby maintaining its accuracy and relevance over time. Additionally, exploring hybrid models that combine convolutional neural networks with transformers or integrating multi-modal learning approaches that utilize different types of data could further enhance the model's accuracy and robustness.

6 Conclusion

This paper proposed E2E-Swin-Unet++, a novel model that incorporates thyroid gland information to enhance PTMC segmentation accuracy. The model leverages a dual decoder architectures, with the first decoder providing thyroid features to the second, leading to significant improvements in segmentation performance. Evaluation results demonstrate that E2E-Swin-Unet++ outperforms existing models. Ablation studies further confirm the importance of incorporating thyroid features, as their removal resulted in substantial performance drops, validating our design choice. Furthermore, time assessment results indicate that E2E-Swin-Unet++ also holds potential for real-time applications in clinical settings, such as AI-assisted decision-making during RFA surgeries.

References

- [1] Shiva Dideban, Alireza Abdollahi, Alipasha Meysamie, Shokouh Sedghi, and Mona Shahriari. Thyroid papillary microcarcinoma: etiology, clinical manifestations, diagnosis, follow-up, histopathology and prognosis. *Iranian journal of pathology*, 11(1):1, 2016.
- [2] Krzysztof Kaliszewski, Dorota Diakowska, Marta Rzeszutko, Łukasz Nowak, Michał Aporowicz, Beata Wojtczak, Krzysztof Sutkowski, and Jerzy Rudnicki. Risk factors of papillary thyroid microcarcinoma that predispose

- patients to local recurrence. *Plos one*, 15(12):e0244930, 2020.
- [3] Stella Bernardi, Andrea Palermo, Rosario Francesco Grasso, Bruno Fabris, Fulvio Stacul, and Roberto Cesaro. Current status and challenges of us-guided radiofrequency ablation of thyroid nodules in the long term: a systematic review. *Cancers*, 13(11):2746, 2021.
- [4] Lisa A Orloff, Julia E Noel, Brendan C Stack Jr, Marika D Russell, Peter Angelos, Jung Hwan Baek, Kevin T Brumund, Feng-Yu Chiang, Mary Beth Cunnane, Louise Davies, et al. Radiofrequency ablation and related ultrasound-guided ablation technologies for treatment of benign and malignant thyroid disease: An international multidisciplinary consensus statement of the american head and neck society endocrine surgery section with the asia pacific society of thyroid surgery, associazione medici endocrinologi, british association of endocrine and thyroid surgeons, european thyroid association, italian society of endocrine surgery units, korean society of thyroid radiology, latin american thyroid society, and thyroid nodules therapies association. *Head & neck*, 44(3):633–660, 2022.
- [5] Krzysztof Kaliszewski, Dorota Diakowska, Beata Wojtczak, Zdzisław Forkasiewicz, Dominika Pupka, Łukasz Nowak, and Jerzy Rudnicki. Which papillary thyroid microcarcinoma should be treated as “true cancer” and which as “precancer”? *World Journal of Surgical Oncology*, 17:1–8, 2019.
- [6] Alireza Mohammadkarim, Manijhe Mokhtari-Dizaji, Ali Kazemian, and Hazhir Saberi. Hemodynamic analysis of radiation-induced damage in common carotid arteries by using color doppler ultrasonography. *Ultrasonography*, 37(1):43, 2018.
- [7] Rakesh Mistry, Christopher Hillyar, Anjan Nibber, Thushanth Sooriyamoorthy, and Nirmal Kumar. Ultrasound classification of thyroid nodules: a systematic review. *Cureus*, 12(3), 2020.
- [8] Bernd B Frericks, Jörg P Ritz, Thomas Albrecht, Steffi Valdeig, Andrea Schenk, Karl-Jürgen Wolf, and Kai Lehmann. Influence of intrahepatic vessels on volume and shape of percutaneous thermal ablation zones: in vivo evaluation in a porcine model. *Investigative radiology*, 43(4):211–218, 2008.
- [9] Woo Kyoung Jeong, Jung Hwan Baek, Hyunchul Rhim, Yoon Suk Kim, Min Sook Kwak, Hyun Jo Jeong, and Ducky Lee. Radiofrequency ablation of benign thyroid nodules: safety and imaging follow-up in 236 patients. *European radiology*, 18:1244–1250, 2008.
- [10] Samir Khan and Takehisa Yairi. A review on the application of deep learning in system health management. *Mechanical Systems and Signal Processing*, 107:241–265, 2018.
- [11] Risheng Wang, Tao Lei, Ruixia Cui, Bingtao Zhang, Hongying Meng, and Asoke K Nandi. Medical image segmentation using deep learning: A survey. *IET Image Processing*, 16(5):1243–1267, 2022.
- [12] Fausto Milletari, Nassir Navab, and Seyed-Ahmad Ahmadi. V-net: Fully convolutional neural networks for volumetric medical image segmentation. In *2016 fourth international conference on 3D vision (3DV)*, pages 565–571. Ieee, 2016.

- [13] Zongwei Zhou, Md Mahfuzur Rahman Siddiquee, Nima Tajbakhsh, and Jianming Liang. Unet++: A nested u-net architecture for medical image segmentation. In *Deep Learning in Medical Image Analysis and Multimodal Learning for Clinical Decision Support: 4th International Workshop, DLMIA 2018, and 8th International Workshop, ML-CDS 2018, Held in Conjunction with MICCAI 2018, Granada, Spain, September 20, 2018, Proceedings 4*, pages 3–11. Springer, 2018.
- [14] Ozan Oktay, Jo Schlemper, Loic Le Folgoc, Matthew Lee, Mattias Heinrich, Kazunari Misawa, Kensaku Mori, Steven McDonagh, Nils Y Hammerla, Bernhard Kainz, et al. Attention u-net: Learning where to look for the pancreas. *arXiv preprint arXiv:1804.03999*, 2018.
- [15] Zhengxin Zhang, Qingjie Liu, and Yunhong Wang. Road extraction by deep residual u-net. *IEEE Geoscience and Remote Sensing Letters*, 15(5):749–753, 2018.
- [16] Steven Guan, Amir A Khan, Siddhartha Sikdar, and Parag V Chitnis. Fully dense unet for 2-d sparse photoacoustic tomography artifact removal. *IEEE journal of biomedical and health informatics*, 24(2):568–576, 2019.
- [17] Junde Wu, Wei Ji, Yuanpei Liu, Huazhu Fu, Min Xu, Yanwu Xu, and Yueming Jin. Medical sam adapter: Adapting segment anything model for medical image segmentation. *arXiv preprint arXiv:2304.12620*, 2023.
- [18] Haifan Gong, Guanqi Chen, Ranran Wang, Xiang Xie, Mingzhi Mao, Yizhou Yu, Fei Chen, and Guanbin Li. Multi-task learning for thyroid nodule segmentation with thyroid region prior. In *2021 IEEE 18th international symposium on biomedical imaging (ISBI)*, pages 257–261. IEEE, 2021.
- [19] Alexey Dosovitskiy, Lucas Beyer, Alexander Kolesnikov, Dirk Weissenborn, Xiaohua Zhai, Thomas Unterthiner, Mostafa Dehghani, Matthias Minderer, Georg Heigold, Sylvain Gelly, et al. An image is worth 16x16 words: Transformers for image recognition at scale. *arXiv preprint arXiv:2010.11929*, 2020.
- [20] Ashish Vaswani, Noam Shazeer, Niki Parmar, Jakob Uszkoreit, Llion Jones, Aidan N Gomez, Łukasz Kaiser, and Illia Polosukhin. Attention is all you need. *Advances in neural information processing systems*, 30, 2017.
- [21] Hu Cao, Yueyue Wang, Joy Chen, Dongsheng Jiang, Xiaopeng Zhang, Qi Tian, and Manning Wang. Swin-unet: Unet-like pure transformer for medical image segmentation. In *European conference on computer vision*, pages 205–218. Springer, 2022.
- [22] Ze Liu, Yutong Lin, Yue Cao, Han Hu, Yixuan Wei, Zheng Zhang, Stephen Lin, and Baining Guo. Swin transformer: Hierarchical vision transformer using shifted windows. In *Proceedings of the IEEE/CVF international conference on computer vision*, pages 10012–10022, 2021.
- [23] Mohammad Hesam Hesamian, Wenjing Jia, Xiangjian He, and Paul Kennedy. Deep learning techniques for medical image segmentation: achievements and challenges. *Journal of digital imaging*, 32:582–596, 2019.
- [24] Zhuhuang Zhou, Shuicai Wu, Chiao-Yin Wang, Hsiang-Yang Ma, Chung-Chih Lin, and Po-Hsiang Tsui. Monitoring radiofrequency ablation using real-time ultrasound nakagami imaging combined with frequency and temporal compounding techniques. *PLoS One*, 10(2):e0118030, 2015.

APPENDIX

A Hyperparameters

Table below provides a list of hyper-parameters used in the experiments.

Table 4: Hyper-parameters.

Parameter	Value
BATCH SIZE	32
IMG SIZE	224
DROP RATE	0.0
LABEL SMOOTHING	0.1
PATCH SIZE	4
EMBED DIM	96
DEPTHS	[2, 2, 6, 2]
DECODER DEPTHS	[2, 2, 6, 2]
NUM HEADS	[3, 6, 12, 24]
WINDOW SIZE	7
MLP RATIO	4.0
EPOCHS	300
WARMUP EPOCHS	20
WEIGHT DECAY	0.05
CLIP GRAD	5.0
ACCUMULATION STEPS	0
DECAY EPOCHS	30
DECAY RATE	0.1
BETAS	(0.9, 0.999)
MOMENTUM	0.9
COLOR JITTER	0.4
REPROB	0.25
RECOUNT	1.0
MIXUP	0.8
CUTMIX	1.0
MIXUP PROB	1.0
MIXUP SWITCH_PROB	0.5
SEED	0